Journal of the Korean Ceramic Society
Vol. 51, No. 3, pp. 162~169, 2014.

http://dx.doi.org/10.4191/kcers.2014.51.3.162

# Sonophotocatalytic Performance of $Bi_2Se_3$-Graphene/$TiO_2$ Hybrid Nanomaterials Synthesized with a Microwave-assisted Method

**Lei Zhu, Sun-Bok Jo, Shu Ye, Kefayat Ullah, and Won-Chun Oh*,†**

*Department of Advanced Materials Science & Engineering, Hanseo University, Chungnam 356-706, Korea*
(Received March 7, 2014; Revised April 24, 2014; Accepted May 3, 2014)

**ABSTRACT**

This paper introduces a microwave-assisted synthesis method to prepare hybrid $Bi_2Se_3$-GR/$TiO_2$ nanocomposites, which exhibit superior properties over single component materials. The as-prepared composites were characterized by XRD, UV-vis absorbance spectra, SEM,TEM, EDX, and BET analyses, revealing uniform covering of the graphene nanosheet with $Bi_2Se_3$ and $TiO_2$ nanocrystals. For visible light photocatalysis of Rh.B, a significant enhancement in the reaction rate was consequently observed with $Bi_2Se_3$-GR/$TiO_2$ composites. The degradation rate($k_{app}$) obtained for sonophotocatalysis was $6.8\times 10^{-3}$ $min^{-1}$, roughly 2.2 times better than that of VL photocatalysis under higher concentrations of Rh.B. The sonophotocatalysis was faster due to greater formation of reactive radicals as well as an increase of the active surface area of the $Bi_2Se_3$-GR/$TiO_2$ composites. The high activity is attributed to the synergetic effects of high charge mobility and red shift of the absorption edge of $Bi_2Se_3$-GR/$TiO_2$.

***Key words : Microwave-assisted synthesis, Visible light, Sonophotocatalysis, Graphene hybrid, $Bi_2Se_3$***

## 1. Introduction

$TiO_2$ is a widely used photocatalyst due to its good photocatalytic activity, high chemical stability, inexpensiveness, high oxidation capability, and non-toxicity.[1] Modifying $TiO_2$ photocatalysts to enhance light absorption and photocatalytic activity under visible light irradiation has become the main research direction in this areain recent years. To improve the response of $TiO_2$ to visible light, transition metal[2] or non-metal atom[3] doped $TiO_2$ and metal complex[4] sensitized $TiO_2$ have been developed. An alternative approach for achieving this objective is to couple $TiO_2$ by using a narrow band gap semiconductor with a higher conduction band (CB) than that of $TiO_2$. In this sensitized $TiO_2$, charge injection from the CB of a narrow band gap semiconductor to that of $TiO_2$ can lead to efficient and longer charge separation by minimizing the electron–hole recombination. Transition metal sulfides are widely used in the preparation of doping photocatalysts. Several methods for photosensitization of $TiO_2$ by $M_xS_y$ nano particles for heterogeneous photocatalysis have been reported,[5] including approaches using CdS,[6,7] $Bi_2S_3$,[7] and ZnS.[8] In this context, 3d transition metal disulfides have drawn considerable attention because of their technological importance in catalysis, lubrications, battery fabrication, cathode materials for high energy density batteries, and other applications.[9,10] $Bi_2Se_3$ has a smaller band gap (0.3 eV)[11] than $TiO_2$ (3.2eV), thereby making it possible to use $Bi_2Se_3$ as a photosensitizer for $TiO_2$ by injecting the conduction band electrons from $Bi_2Se_3$ to $TiO_2$.

Since its discovery in 2004, graphene, aflatmono layer of hexagonally arrayed $sp^2$-bonded carbon atoms tightly packed into at wo-dimensional (2D) honeycomb lattice, has been the major focus of recentre search due to its outstanding mechanical, electrical, thermal, and optical properties,[12,13] giving rise to potential applications in many different areas. Graphene-based composite materials have attracted much attention as recent studies have shown usefulness in electronics, photocatalysis, and photovoltaic devices.[14-16] Graphene is able to enhance charge transport in a multitude of devices owing to its unique structure: an abundance of delocalized electrons within its conjugated $sp^2$-bonded graphitic carbon network enables excellent conductivity. To date, various metals-RGO and metal oxide-RGO nano composites including RGO combined with palladium, silver, gold, $TiO_2$, and CdSe particles have been reported.[17-21]

Regarding the degradation mechanisms of photocatalysis, a number of studies have indicated that OH• is formed on the photocatalyst during the photochemical reactions. A combination of photocatalytic and ultrasonic irradiation, i.e. so-called sonophotocatalysis, appears to enhance the degradation ratio of organic pollutants due to increased generation of OH•. Notably, sonophotocatalysis is reported to have a positive effect on the degradation ratio of hazardous chemical substances[22] and water pollutant.[23] Among the results of these studies, ultrasound was shown to have a synergistic effect on the photode gradation of salicylic acid and formic acid,[22] while the detailed mechanisms have not been clarified yet.

†Corresponding author : Won-Chun Oh
E-mail : wc_oh@hanseo.ac.kr
Tel : +82-41-660-1337 Fax : +82-41-688-3352

It is well known that the synthesis of nanomaterials with uniform size, shape, and high crystallinity is one of the important challenging problems. There are various kinds of synthesis methods available for the preparation of nanomaterials such as hydrothermal, microwave synthesis, sol–gel, micro-emulsion, and polyol techniques. As compared to common methods, the microwave synthesis technique provides such advantages as a very short reaction time, small particle size, and narrow particle size distribution, and it is a high purity method suitable for the preparation of polycrystalline products.[24] Microwave heating is delivered to the surface of the material by radiant and/or convection heating, and is transferred to the bulk of the material via conduction. The microwave energy is delivered directly to the material through molecular interactions with the electromagnetic field. Heat can be generated through volumetric heating because microwaves can penetrate the material and supply energy. [25]

Upon this background, the aim of this work is to synthesize composite sonophotocatalysts via a microwave-assisted synthesis method and study the degradation of Rh.B by means of visible light photocatalysis and sonophotocatalysis. A particular goal of this study is to develop a suitable catalyst to obtain the maximal degradation rate of Rh.B dye compounds from aqueous solutions. The influence of $Bi_2Se_3$ and graphene on the structural behavior of the $TiO_2$ samples is studied by SEM, EDX, XRD, BET, TEM, and UV-vis DRS. The factors contributing to the improved photocatalytic activity of the $Bi_2Se_3$-GR/$TiO_2$ composites are also discussed.

## 2. Experimental Procedure

### *2.1. Materials and reagents*

Ethylene glycoland anhydrous ethanol were purchased from Dae Jung Chemical Co. (Korea). Bismuth nitrate ($Bi(NO_3)_3 \cdot 5H_2O$ ), selenium (Se) metal powder, and ammonium hydroxide ($NH_4OH$, 28%) were purchased from Dae Jung Chemicals &Metal Co., Ltd, Korea. Anhydrous purified sodium sulfite ($Na_2SO_3$, 95%) was purchased from Duksan Pharmaceutical Co., Ltd, Korea. Titanium (IV) *n*-but oxide (TNB, $C_{16}H_{36}O_4Ti$ ) was purchased from Kanto Chemical Company (TOKYO, Japan) as a titanium source for the preparation of $TiO_2$ and graphene/$TiO_2$ composites. Rh.B ($C_{28}H_{31}ClN_2O_3$, 99.99+%) was used as model pollutant and purchased from Samchun Pure Chemical Co., Ltd, Korea. All chemicals were used without further purification and all experiments were carried out using distilled water.

### *2.2. Synthesis of $Bi_2Se_3$-GR/$TiO_2$ nano composite sonophotocatalysts*

The direct growth of $TiO_2$ precursors on a grapheme nanosheet and absorbed on them were achieved in previous research.[26] Graphite oxide (GO) was prepared from graphite according to the Hummers-Offeman method reported in earlier studies by the author.[27,28] In a typical synthesis procedure, about 300 mg of GO was dispersed in 350 ml of distilled water and then exfoliated to generate graphene oxide nanosheets (GONS) by ultra sonication for 1 h using a digital sonifer.[29] $TiO_2$ precursors were prepared with molarratios of ethanol : $H_2O$ : TNB = 35 : 15 : 4, and then added to the above solution and stirred for 6 h at 353 K. The final products were filtered and washed repeatedly with distilled water and ethanol and then vacuum dried at 373 K. The dried catalyst was then ground in a ball mill and calcined at 773 K for 3 h to yield a graphene-$TiO_2$ composite.

The $Bi_2Se_3$-GR/$TiO_2$ nanocomposite was prepared via a precipitation process using $Bi(NO_3)_3 \cdot 5H_2O$ and $Na_2SeSO_3$ as precursors. First, $Na_2SO_3$ (5 g) and selenium powder were dissolved in 30 mL of distilled water and refluxed for 1 h to form a $Na_2SeSO_3$ solution. A defined amount of as-prepared graphene-$TiO_2$ powder and 8 mL of $NH_4OH$ were then dissolved in the above solution. Subsequently, 0.5 Mm $Bi(NO_3)_3 \cdot 5H_2O$ were added and mixed together via stirring for several minutes and the resultant solution was transferred into a 120 mL reaction vessel and placed in a conventional microwave oven (Samsung, RE-406B 700 W). The solution was then irradiated by microwave at full power for 10 sec on and 10 sec off for 300 seconds, and cooled at room temperature and washed several timed with hot water and transferred into a dry oven. For comparison, pure $TiO_2$,[22] $Bi_2Se_3$-$TiO_2$, and GR-$TiO_2$[26] were prepared with slight modification to the procedure. The preparation conditions and nomenclatures are listed in Fig. 1 and Table 1.

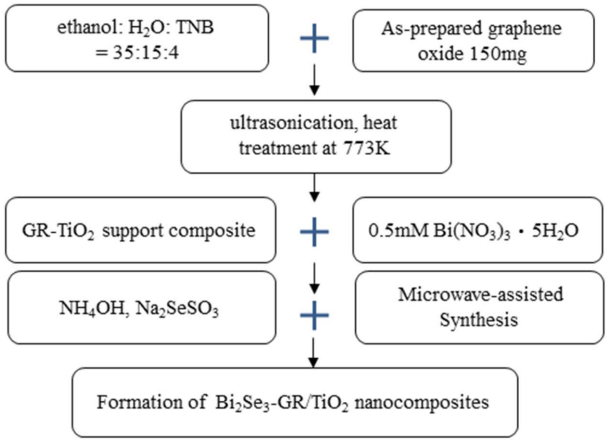


**Fig. 1.** Flow chart of preparation of $Bi_2Se_3$-GR/$TiO_2$ nanocomposites.

**Table 1.** Nomenclature of the As-prepared Samples

| Preparation method | Nomenclature |
|---|---|
| Graphene oxide via Hummers-Offeman method | GO |
| Ethanol: $H_2O$: TNB + Ultrasonic | Nanoscale $TiO_2$ |
| GO + Ethanol: $H_2O$: TNB + Ultrasonic + Heat treatment | GR-$TiO_2$ |
| $Bi(NO_3)_3 \cdot 5H_2O$+$Na_2SeSO_3$+ $TiO_2$ | $Bi_2Se_3$-$TiO_2$ |
| $Bi(NO_3)_3 \cdot 5H_2O$+$Na_2SeSO_3$+ GR-$TiO_2$+ Microwave | $Bi_2Se_3$-GR/$TiO_2$ |

### *2.3. Characterization of composite sonophotocatalysts*

The crystallographic structures of the composite sonophotocatalysts were obtained by XRD (Shimatz XD-D1, Japan) at room temperature with Cu Kα radiation (λ = 0.154056 nm) and a graphite monochromator, operated at 40 KV and 30 mA. UV-vis absorbance spectra were measured between 300 nm and 800 nm using a UV-vis spectrophotometer (Neosys-2000). The morphologies of the photocatalysts were analyzed at 3.0 keV by a SEM (JSM-5200 JOEL, Japan) equipped with an X-ray analysis (EDX) energy dispersive analysis system. Transmission electron microscopy (TEM, JEOL, JEM-2010, Japan) with an accelerating voltage of 200 kV was used to examine the size and distribution of the photocatalysts. The BET surface areas of the sonophotocatalysts were determined through nitrogen adsorption at 77 K using a BET analyzer (Monosorb, USA). All samples were degassed at 623 K before measurement. The UV-vis spectra for the Rh.B solution degraded by as-prepared composite sonophotocatalysts under visible light irradiation were recorded using a UV-Vis (Optizen Pop Mecasys Co., Ltd., Korea) spectrometer.

### *2.4. Measurement of sonophotocatalytic activities*

Photocatalytic activity of the as-prepared composites onophotocatalysts was evaluated by the degradation of the Rh.B solution under irradiation of visible light (35 W, λ > 420 nm). In an ordinary photocatalytic test performed at room temperature, 0.03 g of the composite sonophotocatalyst was added to 50 mL of $3.0 \times 10^{-5}$ mol/L Rh.B solution. In addition, the sonophotocatalytic activities were determined using Rh.B decomposition in an aqueous solution under visible light combined with ultrasonic generators (Ultrasonic Processor VCX 750, Korea) operated at a dixed frequency of 20 kHz and output power of 750 W through manual adjustment. The initial Rh.B concentration was chosen as $2.0 \times 10^{-5}$ mol/L. Before turning on the light source, the solution mixed with the composite was magnetically agitated for 30 mins in the dark, allowing the adsorption/desorption equilibrium to be reached. The first sample was removed at the end of the dark adsorption period (just before the light was turned on), in order to determine the Rh.B concentration in the solution after dark adsorption, which was hereafter considered as the initial concentration ($C_{ads}$). Samples were then withdrawn regularly from the reactor in the order of 30, 60, 90, and 120 min. The clean transparent solution was analyzed using a UV-vis spectrophotometer (Optizen POP) at wavelength from 250 nm to 800 nm.

## 3. Results and Discussion

### *3.1. Structural analysis*

Fig. 2 shows the X-ray diffraction patterns of the as-prepared pure $TiO_2$, $Bi_2Se_3$, GR-$TiO_2$, and $Bi_2Se_3$-GR/$TiO_2$ composite sonophotocatalysts. According to the results, (101), (004), (200), (105), (211), and (204) crystalplanes originated from the anatase $TiO_2$ phase (JCPDS file, No. 21-1272),

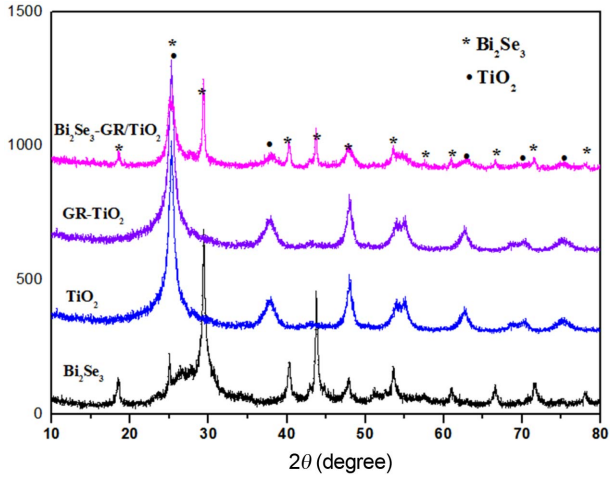


**Fig. 2.** XRD analysis of pure $Bi_2Se_3$, $TiO_2$, GR-$TiO_2$, and $Bi_2Se_3$-GR/$TiO_2$ composite.

while all of the reflection peaks of the XRD pattern can be indexed to rhombohedral (hexagonal) $Bi_2Se_3$, with calculated lattice parameters of $a = 4.1716$ Å and $c = 27.696$ Å. These values correspond to published lattice parameters of $a = 4.1396$ Å and $c = 28.636$ Å (JCPD33-214).[30] No reflection peaks of impurities are observed, indicating high purity of the products. However, no signal for any other phases related to GO (001) or graphene (002) can be detected in the $Bi_2Se_3$-GR/$TiO_2$ composite. According to Ref. 15, GO can be reduced to graphene during the reaction and the synthesized graphene sheets can restack to form poorly ordered graphite along the stacking direction. Earlier studies have shown that if the regular stacking of GO or graphite is broken, for example, by exfoliation, their diffraction peaks may also become weak or even disappear.[31]

### *3.2. Surface characteristics and elemental analysis*

Themorphologies of the prepared $TiO_2$, GR-$TiO_2$, and $Bi_2Se_3$-GR/$TiO_2$ composites are shown in Fig. 3. The agglomeration size of the synthesized $TiO_2$ nanostructures can be estimated from Fig. 3(a), and it is clear that the nanoparticle shape in all three samples is spherical. The above observation shows the existence of $TiO_2$ embedded graphene sheets, and this is also revealed in the SEM image in Fig. 3(b). The graphene in the nanocomposites (GR-$TiO_2$) also shows a dominant $TiO_2$ spherical morphology and particle size. The prepared $Bi_2Se_3$-GR/$TiO_2$ composite meanwhile shows a favorable morphology with $Bi_2Se_3$ and $TiO_2$ particles well-dispersed on a single layered grapheme nano sheet, but with a slight tendency to agglomerate. The agglomeration may be due to the very small crystal particle size, which facilitates agglomeration of particles due to weak surface forces. EDX was carried out to probe the composition and element weight percent of the attached nanoparticles in the $Bi_2Se_3$-GR/$TiO_2$ composite. The spectrum is shown in Fig. 3(d) for pure $TiO_2$, $Bi_2Se_3$/$TiO_2$, and $Bi_2Se_3$-GR/$TiO_2$ composites. The data obtained from EDX

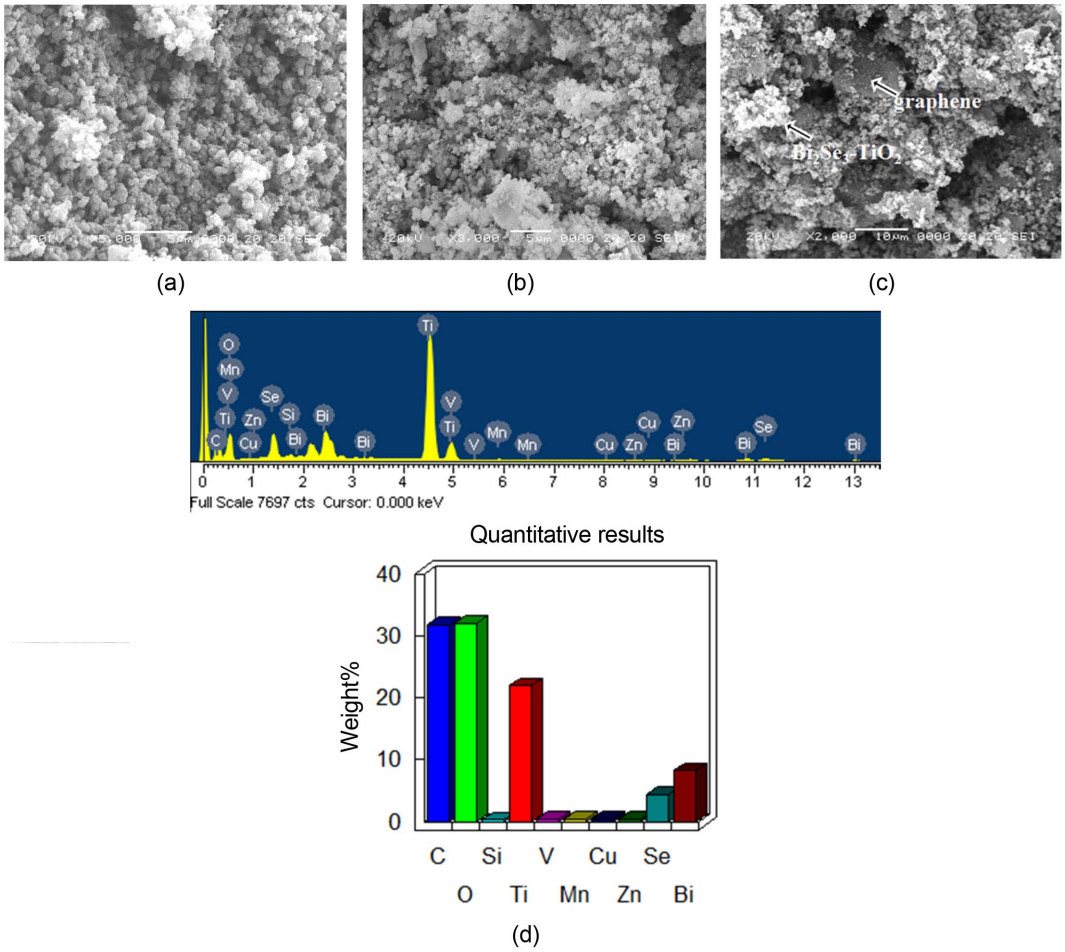


**Fig. 3.** SEM micrographs of as-prepared samples:(a) $TiO_2$, (b) GR-$TiO_2$, (c) $Bi_2Se_3$-GR/$TiO_2$, and (d) EDX elemental microanalysis and element weight % of $Bi_2Se_3$-GR/$TiO_2$ composite.

**Table 2.** EDX Elemental Microanalysis and BET Surface Areas of As-prepared Samples

| Sample name | C (%) | O (%) | Ti (%) | Se(%) | Bi(%) | others | BET ($m^2$/g) |
|---|---|---|---|---|---|---|---|
| $TiO_2$ | - | 45.22 | 54.78 | - | - | - | 18.95 |
| $Bi_2Se_3$-$TiO_2$ | - | 52.12 | 33.57 | 4.84 | 9.47 | | 25.61 |
| GR-$TiO_2$ | 20.84 | 44.11 | 35.05 | - | - | - | 59.89 |
| $Bi_2Se_3$-GR/$TiO_2$ | 31.49 | 34.23 | 21.73 | 3.89 | 7.28 | 1.38 | 52.73 |

analyses of the as-prepared composites are listed in Table 2. The main elements as presence of strong Ti and O peaks of 4.51 keV, 4.92 keV, and 0.52 keV were observed. Elements C, Bi, and Sewere also observed and some impure elements such as Mn, Si, V, Zn, and Cu existed in the $Bi_2Se_3$-GR/$TiO_2$ composites. This indicates that in addition to $TiO_2$ particles $Bi_2Se_3$ was also present.

TEM images of GR-$TiO_2$ and $Bi_2Se_3$-GR/$TiO_2$ nanocomposites with different magnification are presented in Fig. 4. The composite exhibited a uniform size distribution and the $TiO_2$ particles are cubic-shaped with an average size of 10 nm. The black dots in the $Bi_2Se_3$-GR/$TiO_2$ matrix are attributed to the accumulation and high electron density of $Bi_2Se_3$ nanoparticles with a size range from15 nm to 20 nm. The results indicate that the surface of the grapheme nano sheet was uniformly distributed with $Bi_2Se_3$ and $TiO_2$ particles in contact with each other.

In order to check the visible photo-response of the pure $TiO_2$, GR-$TiO_2$, and $Bi_2Se_3$-GR/$TiO_2$ composites, UV-vis absorption spectra are presented in Fig. 5. As expected, the spectra obtained from the pure $TiO_2$ and GR-$TiO_2$ composites shows that $TiO_2$ mainly absorbs ultraviolet light with absorption wavelength below 400 nm. Compared with pure $TiO_2$, a shift of the intense absorbance edge of GR-$TiO_2$ and $Bi_2Se_3$-GR/$TiO_2$ composites towards the visible light region was observed and the absorption edge was located at approximately 738 nm. The absorbance spectra of the as-formed $Bi_2Se_3$-GR/$TiO_2$ composite show intense absorption and dis-

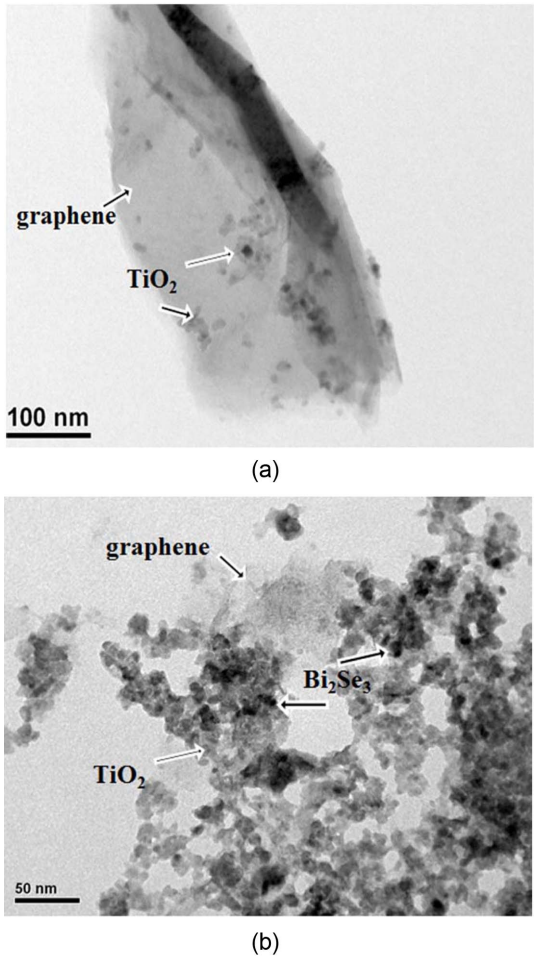


**Fig. 4.** TEM micrographs of as-prepared composites: (a) GR-$TiO_2$ and (b) $Bi_2Se_3$-GR/$TiO_2$.

play a red-shift absorption onset compared with both $TiO_2$ and GR-$TiO_2$.

### *3.3. Porous structure characteristics*

The specific surface areas (BET) of the pure $TiO_2$, $Bi_2Se_3$/$TiO_2$, GR-$TiO_2$, and $Bi_2Se_3$-GR/$TiO_2$ composites are listed in Table 2. The BET value decreased from 59.89 $m^2/g$ for GR-$TiO_2$ to 52.73 $m^2/g$ for $Bi_2Se_3$-GR/$TiO_2$. It is surmised that the $TiO_2$ and $Bi_2Se_3$ nanoparticles were introduced into the pores of the graphene, which decreased the BET surface area.The GR-$TiO_2$ has the largest area, which can affect the adsorption reaction. The surface area of the $Bi_2Se_3$-$TiO_2$ photocatalysts was 25.61 $m^2/g$, which was higher than that of pure $TiO_2$ sample. This might be attributable to the formation of mesopores and macro pores when the $Bi_2Se_3$ nanoparticles were distributed on the surface of $TiO_2$.

### *3.4. Visible light photocatalysis of Rh.B*

Fig. 6(a) shows the photocatalytic activity of pure $TiO_2$, $Bi_2Se_3$-$TiO_2$, GR-$TiO_2$, and $Bi_2Se_3$-GR/$TiO_2$ composite photocatalysts evaluated by the decomposition of Rh.B solution under visible light irradiation for 120 min. As shown in

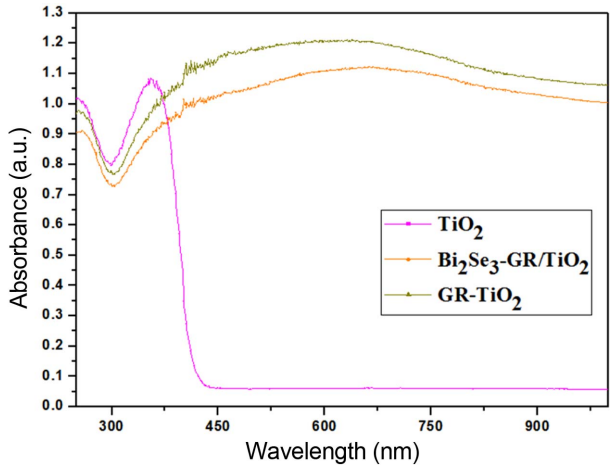


**Fig. 5.** UV-vis adsorption spectra of pure $TiO_2$, GR-$TiO_2$, and $Bi_2Se_3$-GR/$TiO_2$ composite.

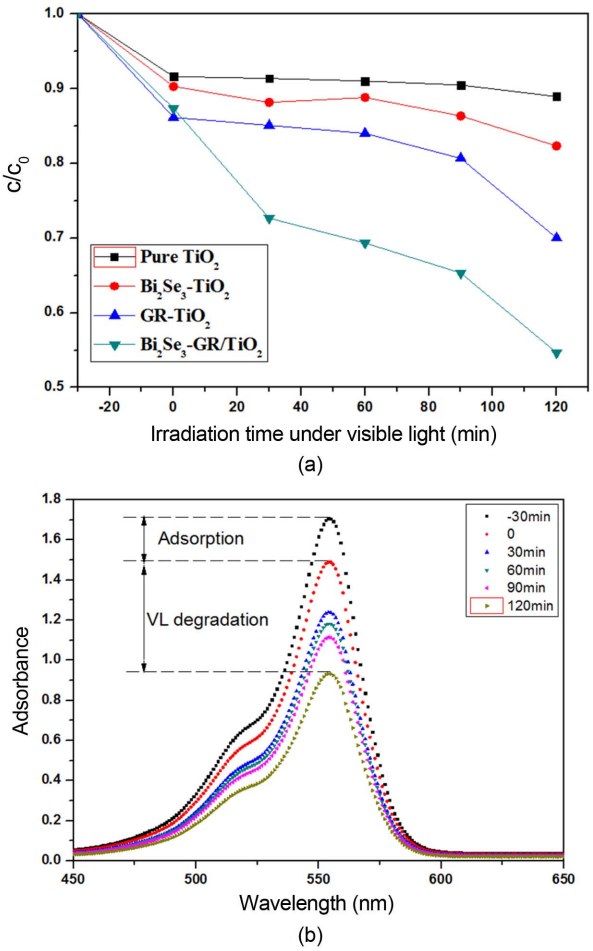


**Fig. 6.** (a) Degradation of Rh.B dye ($3 \times 10^{-5}$mol/L, 50 mL) with different samples (0.03 g) and (b) UV/V is spectra of Rh.B concentration against the $Bi_2Se_3$-GR/$TiO_2$ composite under visible light for 120 min.

Fig. 6(b), the absorbance values for the $Bi_2Se_3$-GR/$TiO_2$ composite decreased with an increase of visible light irradiation time. The $Bi_2Se_3$/$TiO_2$ composite showed more remarkable

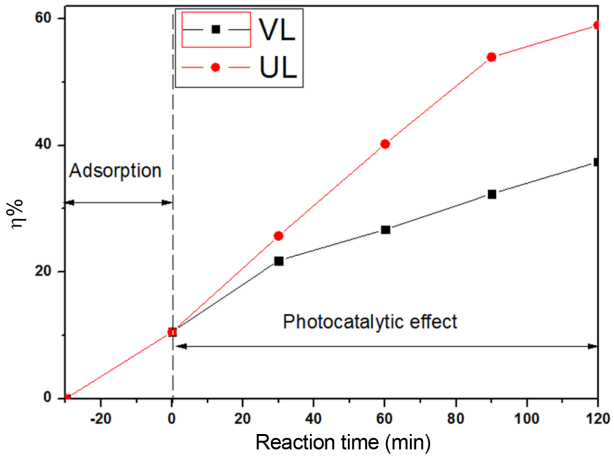


**Fig. 7.** Degradation efficiency of Rh.B solution by $Bi_2Se_3$-GR/$TiO_2$ composite under irradiation of visible light (VL) and ultrasonic combined visible light (UL). The concentration of organic dyes is $2 \times 10^{-5}$M; the amount of $Bi_2Se_3$-GR/$TiO_2$ composite is 0.03 g.

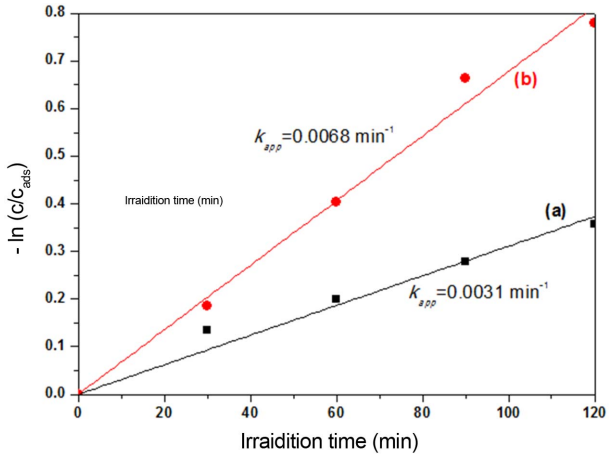


**Fig. 8.** Apparent first-order linear transforms $-\ln(c/c_{ads})$ vs. $t$ of Rh.B degradation on $Bi_2Se_3$-GR/$TiO_2$ composite under visible light (a) and ultrasonic combined visible light (b) irradiation. The concentration of Rh.B solution is $2 \times 10^{-5}$ M; the amount of catalyst is 0.03 g.

and faster adsorption capacity of Rh.B solution than pristine $TiO_2$. The adsorption effect of GR-$TiO_2$ is better than that of any other samples due to the relatively higher surface area. The photocatalytic degradation of the Rh.B solution with the $Bi_2Se_3$-GR/$TiO_2$ composite was better than that of the other composites: 45.4% of the Rh.B solution with high concentration was removed after visible light irradiation for 120 min. As mentioned above with regard to surface characteristics, the favorable morphology could play an important role in efficiently shuttling visible light photoinduced electrons generated from $Bi_2Se_3$ into the conduction band of $TiO_2$.[32]

### *3.5. Sonophotocatalysis of Rh.B*

It has been suggested that the combination of photocatalysis and sonolysis is more effective in dye degradation. Ultrasound may promote the rate of photocatalytic degradation by modifying the deaggregation of the catalyst and thereby increasing its active surface area. Thus, in order to obtain the sonophotocatalytic activity for the $Bi_2Se_3$-GR/$TiO_2$ composite, the concentration was increased to $2 \times 10^{-5}$ M. The sonophotocatalysis results are shown in Fig. 7. The results show that the Rh.B degradation efficiency of visible light photocatalysis for 120 min was 37% while that of sonophotocatalysis for the same time was 59%. This is due to the photocatalyst being excited by ultrasound-induced luminescence, which has a wide wavelength and increased production of hydroxyl radicals (.OH) in the reaction mixture.[33] It is also observed that the prepared $Bi_2Se_3$-GR/$TiO_2$ composite has high degradation activity not only under visible light but also under ultrasonic. The sonophotocatalysis of Rh.B by the $Bi_2Se_3$-GR/$TiO_2$ composite obeys pseudo-first-order kinetics:

$$-dc/dt = k_{app}c$$

Integration of the above equation (with the restriction of $c=c_{ads}$ at $t=0$, with $c_{ads}$ being the initial concentration in the bulk solution after dark adsorption and $t$ the reaction time) leads to the following expected relation:

$$-\ln(c/c_{ads}) = k_{app}t$$

where$c$ and $c_{ads}$ are the reactant concentration at time $t = t$ and $t = 0$, respectively, and $k_{app}$ and $t$ are the apparent reaction rate constant and time, respectively. According to the equation, a plot of $-\ln(c/c_{ads})$ versus $t$ will yield a slope of $k_{app}$. The results are displayed in Fig. 8. The linearity of the plot suggests that the photo degradation reaction approximately follows pseudo-first-order kinetics with $k_{app}$ of 0.0031 min$^{-1}$ and 0.0068 min$^{-1}$ for VL photocatalysis and sonophotocatalysis, respectively.

### *3.6. Proposed sonophotocatalysis mechanism*

The sonophotocatalytic mechanism of dye degradation is extremely complicated. It is likely to involve photolysis, sonolysis, and sonophotocatalysis. In the case of a nanosized $Bi_2Se_3$ and $TiO_2$ nanocrystal line coupled graphene based photcatalyst system, coupling of two such semiconductors has a beneficial role in improving charge separation and extends $TiO_2$ in response to visible light compared with our previous experiment results.[34] A mechanism for the degradation of pollutants on a $Bi_2Se_3$ coupled $TiO_2$ catalyst under visible light irradiation and ultrasonic irradiation is shown in Fig. 9. During the sonophotocatalysis process, the generated electrons in $Bi_2Se_3$ and holes in $TiO_2$ migrate to the conduction band (CB) of $TiO_2$ and the valence band (VB) of $Bi_2Se_3$, respectively. This transfer process is thermo dynamically favorable due to both the CB and VB of $Bi_2Se_3$ lying above that of $TiO_2$. Meanwhile, the generated electrons likely react with dissolved oxygen molecules and pro-

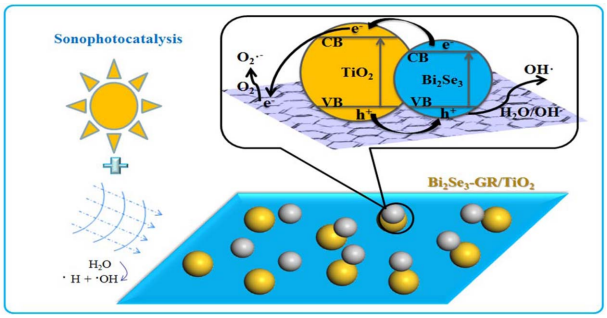


**Fig. 9.** Schematic drawing of separation of generated electrons and holes on the interface of $Bi_2Se_3$-GR/$TiO_2$ composite under ultrasonic irradiation.

duce oxygen peroxide radical $O_2^{\cdot -}$, and the positive charged hole ($h^+$) may react with the $OH^-$ derived from $H_2O$ to form the hydroxyl radical $OH^{\cdot}$. The reactions can be expressed as follows:

$$Bi_2Se_3 + h\upsilon \rightarrow Bi_2Se_3\,(e^-) + Bi_2Se_3\,(h^+) \quad (1)$$
$$TiO_2 + h\upsilon \rightarrow TiO_2(e^-) + TiO_2(h^+) \quad (2)$$
$$\text{Graphene} + h\upsilon \rightarrow \text{Graphene}(e^-) \quad (3)$$
$$TiO_2(e^-) + \text{Graphene} \rightarrow \text{Graphene}(e^-) + TiO_2 \quad (4)$$
$$Bi_2Se_3\,(e^-) + O_2 \rightarrow Bi_2Se_3 + O_2^{\cdot -} \quad (5)$$
$$TiO_2(e^-) + O_2 \rightarrow TiO_2 + O_2^{\cdot -} \quad (6)$$
$$\text{Graphene}(e^-) + O_2 \rightarrow \text{Graphene} + O_2^{\cdot -} \quad (7)$$
$$Bi_2Se_3\,(h^+) + H_2O \rightarrow Bi_2Se_3 + OH^{\cdot} + H^+ \quad (8)$$
$$TiO_2(h^+) + H_2O \rightarrow TiO_2 + OH^{\cdot} + H^+ \quad (9)$$

## 4. Conclusions

In this study, we present the preparation and characterization of a $Bi_2Se_3$-GR/$TiO_2$ nanocomposite via a facile microwave-assisted synthesis method. A typical anatase $TiO_2$ structure and a hexagonal $Bi_2Se_3$ structure can be observed in the XRD patterns. From the SEM morphology, for the $Bi_2Se_3$-GR/$TiO_2$ sample, graphene flakes are readily observed and they are decorated with uniform $Bi_2Se_3$ particles and $TiO_2$ particles. The $Bi_2Se_3$-GR/$TiO_2$ nano composites show an intense absorption and have a red-shift absorption onset compared with both $TiO_2$ and $Bi_2Se_3$/$TiO_2$. According to the excellent dye degradation results, the decrease in the Rh.B concentration can be ascribed to the two kinds of effects between visible light photocatalysis and sonophotocatalysis.

## Acknowledgment

This work was supported by the Research Foundation from Hanseo University in 2013. The authors are grateful to staffs in the University for financial support.

## REFERENCES

1. K. Hashimoto, H. Irie, and A. Fujishima, "$TiO_2$ Photocatalysis: A Historical Overview and Future Prospects," *Jpn. J. Appl. Phys.,* **44** [12] 8269-85 (2005).
2. M. Anpo and M. Takeuchi, "The Design and Development of Highly Reactive Titanium Oxide Photocatalysts Operating under Visible Light Irradiation," *J. Catal.,* **216** [1-2] 505-16 (2003).
3. H. Irie, Y. Watanabe, and K.Hashimoto, "Nitrogen-concentration Dependence on Photocatalytic Activity of $TiO_{2-x}N_x$ Powders," *J. Phys. Chem., B,* **107** [23] 5483-86 (2003).
4. H. Kisch, L. Zang, C. Lange, W. F. Maier, C. Meissner, and D. Angew, "Modified Amorphous Titania— A Hybrid Semiconductor for Detoxification and Current Generation by Visible Light," *Chem. Int. Ed.,* **37** [21] 3034-36 (1998).
5. D. Robert, "Photosensitization of $TiO_2$ by $M_xO_y$ and $M_xS_y$ Nanoparticles for Heterogeneous Photocatalysis Applications," *Catal. Today.,* **122** [1-2] 20-26 (2007).
6. J. C. Kim, J. Choi, Y. B. Lee, J. H. Hong, J. I. Lee, J. W. Yang, W. I. Lee, and N. H. Hur, "Enhanced Photocatalytic Activity in Composites of $TiO_2$ Nanotubes and CdS Nanoparticles," *Chem. Commun.,* **48** 5024–26 (2006).
7. Y. Bessekhouad, D. Robert, and J. V. Weber, "$Bi_2S_3$/$TiO_2$ and CdS/$TiO_2$ Heterojunctions as an Available Configuration for Photocatalytic Degradation of Organic Pollutant," *J. Photochem. Photobiol., A,* **163** [3] 569–80 (2004).
8. V. Štengl, S. Bakardjieva, N. Murafa, V. Houšková , and K. Lang, "Visible-light Photocatalytic Activity of $TiO_2$/ZnS Nanocomposites Prepared by Homogeneous Hydrolysis," *Micropor. Mesopor. Mater.,* **110** [2-3] 370–78 (2008).
9. K. B. Tang, Y. T. Qian, J. H. Zeng, and X. G. Yang, "Solvothermal Route to Semiconductor Nanowires," *Adv. Mater.,***15** [5] 448-50 (2003).
10. R. Luo, X. Sun, L. F. Yan, and W. M. Chen, "Synthesis and Optical Properties of Novel Nickel Disulfide Dendritic Nanostructures," *Chem. Lett.,* **33** 830–31 (2004).
11. K. Kadel, L. Kumari, W. Z. Li, J. Y. Huang, and P. Paula, "Provencio Synthesis and Thermoelectric Properties of $Bi_2Se_3$ Nanostructures," *Nanoscale. Res. Lett.,* **6** [1] 57-63 (2011).
12. J. C. Meyer, A. K. Geim, and M. I. Katsnelson, "The Structure of Suspended Graphene Sheets," *Nature.,* **446** 60-63 (2007).
13. Y. Zhu, S. Murali, W. Cai, X. Li, J. W. Suk, J. R. Pottsand, and R. S. Ruoff, "Graphene and Graphene Oxide: Synthesis, Properties, and Applications," *Adv. Mater.*, **22** [35] 3906-24 (2010).
14. P. V. Kamat, "Graphene Based Nano Architectures. Anchoring Semiconductor and Metal Nanoparticles on a 2-Dimensional Carbon Support," *J. Phys. Chem. Lett.,* **15** 20-27 (2010).
15. H. Zhang, X. Lv, Y. Li, Y. Wang, and J. Li, "$P_{25}$-Graphene Composite as a High Performance Photocatalyst," *ACS Nano.,***4** [1] 380-86 (2010).
16. S. R. Kim, M. K. Parvez, and M. Chhowalla, "UV-reduction of Graphene Oxide and its Application as an Interfacial Layer to Reduce the Back-transport Reactions in Dye-sensitized Solar Cells," *Chem. Phys. Lett.,* **483** [1-3] 124-27 (2009).
17. G. M. Scheuermann, L. Rumi, P. Steurer, W. Bannwarth, and R. Mulhaupt, "Palladium Nanoparticles on Graphite Oxide and its Functionalized Graphene Derivatives as Highly Active Catalysts for the Suzuki–Miyaura Coupling

Reaction," *J. Am. Chem. Soc.,***131** 8262-70 (2009).
18. R. Pasricha, S.Gupta, and A. K. Srivastava, "A Facile and Novel Synthesis of Ag-Graphene-based Nanocomposites," *Small.,* **5** [20] 2253-59 (2009).
19. R. Muszynski, B. Seger, and P. V. Kamat, "Decorating Graphene Sheets with Gold Nanoparticles," *J. Phys. Chem., C*, **112** [14] 5263-66 (2008).
20. J. Sun, H. Zhang, L. H. Guo, and L. X. Zhao, "Two-dimensional Interface Engineering of a Titania–Graphene Nanosheet Composite for Improved Photocatalytic Activity," *ACS Appl. Mater. Interfaces.,* **5** [24] 13035-41 (2013).
21. Y. Lin, K. Zhang, W. Chen, Y. Liu, Z. Geng, J. Zeng, N. Pan, L. Yan, X. Wang, and J. G. Hou,. "Dramatically Enhanced Photoresponse of Reduced Graphene Oxide with Linker-Free Anchored CdSe Nanoparticles," *ACS Nano.,***4** [6] 3033-38 (2010).
22. L. Davydov, E. P. Reddy, P. France, and P. G. Smirniotis, "Sonophotocatalytic Destruction of Organic Contaminants in Aqueous Systems on $TiO_2$ Powders,"*Appl. Catal. B: Environ.*, **32** [1-2] 95–105 (2001).
23. A. B. Pandit, P. R. Gogate, and S. Mujumdar, "Ultrasonic Degradation of 2: 4: 6 Trichlorophenol in Presence of $TiO_2$ Catalyst," *Ultrason. Sonochem.,* **8** [3] 227–31 (2001).
24. K. Ullah, S. Ye, L. Zhu, Z. D. Meng, S. Sarkar, and W. C. Oh, "Microwave Assisted Synthesis of a Noble Metal-graphene Hybrid Photocatalyst for High Efficient Decomposition of Organic Dyes under Visible Light," *Mater. Sci. Eng. B.,* **180** 20-26 (2014).
25. S. Das, A. K. Mukhopadhyay, S. Datta, and D. Basu, "Prospects of Microwave Processing: An Overview," *Bull. Mater . Sci.,* **31** [7] 1-13 (2009).
26. L. Zhu, T. Ghosh, C. Y. Park, Z. D. Meng, and W. C. Oh, "Enhanced Sonocatalytic Degradation of Rhodamine B by Graphene-$TiO_2$ Composites Synthesized by an Ultrasonic-Assisted Method," *Chin. J. Catal.,* **33** [7-8] 1276-83 (2012).
27. T. Ghosh, K. Y. Cho, K. Ullah, V. Nikam, C. Y. Park, Z. D. Meng, and W. C. Oh, "High Photonic Effect of Organic Dye Degradation by CdSe-graphene-$TiO_2$ Particles," *J. Ind. Eng. Chem.,* **19** [3] 797-805 (2013).
28. W. C. Oh and F. J. Zhang, "Preparation and Characterization of Graphene Oxide Reduced from a Mild Chemical Method," *Asian. J. Chem.,* **23** 875-79 (2011).
29. D. Li, M. B. Muller, S. Giljem, and G. G. Wallace, "Processable Aqueous Dispersions of Graphene Nanosheets," *Nat. Nanotechnol.,* **3** 101-05 (2008).
30. Y. Yu, W. T. Sun, Z. D. Hu, Q. Chen, and L. M.Peng, "Oriented $Bi_2Se_3$ Nano Ribbons Film: Structure, Growth, and Photoelectric Properties," *Mater. Chem. Phys.,* **124** [11] 865-69 (2010).
31. D. Cai and M. Song, "Preparation of Fully Exfoliated Graphite Oxide Nanoplatelets in Organic Solvents," *J. Mater. Chem.,* **17** 3678-80 (2007).
32. J. G. Lei, N. Qie, J. Zhou, Y. Y. Hua, and T. H. Ji, "Preparation and Characterization of $TiO_2$ Nanobelts Deposited with $Bi_2Se_3$ Nanoplates," *Mater.Lett.,* **83** 108-11 (2012).
33. C. Berberidou, I. Poulios, and N. P. Xekoukoulotakis, "Sonolytic, Photocatalytic and Sonophotocatalytic Degradation of Malachite Green in Aqueous Solutions," *Appl. Catal. B-Environ.,* **74** [1-2] 63-72 (2007).
34. K. Zhang and W. C. Oh, "Kinetic Study of the Visible Light-induced Sonophotocatalytic Degradation of MB Solution in the Presence of Fe/$TiO_2$-MWCNT Catalyst," *B. Kor. Chem. Soc.,* **31** [6] 1589-95(2010).